Broadband All-Dielectric Magnifying Lens for Far-Field High-Resolution Imaging

Wei Xiang Jiang, Cheng-Wei Qiu, Tian Cheng Han, Qiang Cheng, Hui Feng Ma, Shuang Zhang, and Tie Jun Cui**

The resolution of a conventional optical microscope is constrained to about half wavelength due to the loss of high spatial frequency information carried in the evanescent waves.[1] To overcome the bottleneck, perfect lens, engineered from a slab of ideal negative-refraction medium, has promised to achieve perfect image by magnifying the evanescent waves.[2] For practical realization, a simplified perfect lens, i.e., superlens, was experimentally demonstrated using a thin slab of silver[3] or SiC.[4] However, such 'nearsighted' superlenses cannot be directly used to replace the traditional optical microscope.[5] To project a near-field image into the far-field region, a far-field superlens (FSL), made of slab superlens with periodic corrugations, was presented later to convert evanescent waves partly into propagating waves.[6] To achieve the high resolution imaging in the far-field region more efficiently, hyperlenses which allow magnification of deep subwavelength scale objects have been proposed by using anisotropic materials with hyperbolic dispersions.[7,8] Soon after, cylindrical hyperlenses[9,10] and spherical hyperlens[11] were experimentally demonstrated with a curved periodic stack of metal-dielectric materials. In fact, based on the transformation optics (TO),[12,13] both superlens and hyperlens can be precisely designed.[14] Due to the absorption and narrowband properties, however, such superlenses and hyperlenses are still limited to laboratory and far away from practical applications. To avoid the limitation, a theoretical proposal of modified immersion lens with a magnification factor has been introduced and analyzed,[15] and super-resolution imaging has been demonstrated using the Maxwell fisheye lenses.[16,17] More recently, a far-field time reversal theory has been developed to reach higher imaging resolution,[18–21] but an array of antennas was required.

In this work, we propose an impedance-matched magnifying lens to provide far-field subwavelength imaging, which is thoroughly made of inhomogeneous isotropic dielectrics based on an approximate but accurate simplification from traditional transformation optics. This novel lens may also be perceived as an improved solid immersion lens operating in microwaves, which does not rely on the hyperbolic dispersions or the coupling between evanescent waves and surface plasmons.[2–11] The lens is fabricated with multilayer dielectric plates by drilling air holes. The far-field high resolution imaging of such lens was experimentally demonstrated in a broadband of gigahertz frequencies. Benefitting from the low-loss and broadband properties of the all-dielectric metamaterial, the experimental results show excellent super-resolution performance from 7 to 10 GHz. The modified solid immersion lens is capable of magnifying the sub-wavelength space between two objects, and producing a magnified image at the far field, where the two objects could be distinguished by conventional imaging system. This mechanism may also find unique potentials in far-field high resolution optical imaging. The proposed operation with high resolution may open new avenues towards real-time imaging systems across a wide spectrum of light.

We begin with a strict coordinate transformation shown in **Figures 1**a and 1b, in which a two-fold transformation needs to be carried out for the design of the modified solid immersion lens. The real and virtual spaces are denoted with (x, y, z) and (x', y', z'), respectively. First, a circular region $(r' \le b - \delta)$ in the virtual space is compressed into region I $(r \le a)$ in real space. Second, an annular region $(b - \delta < r' \le b)$ in the virtual space is stretched into region II $(a < r \le b)$ in the real space. Then the far-field pattern of two closely-packed sources (s1 and s2) in the real space will be equivalent to that of two well-separated sources (s1' and s2') in the virtual space, realizing the functionality of modified solid immersion lens.

Using the transformation optics procedure, we obtain the closed-form expressions of material parameters for the modified solid immersion lens (see Supporting Information). In the case of two dimensions under the transverse electric polarization and letting $\delta \to 0$, we derive the required refractive index of the modified solid immersion lens as

$$n(r) = \begin{cases} \frac{b}{a} & r \le a \\ diag\left(0, \frac{b}{r}\right) & a < r \le b. \end{cases} \quad (1)$$

It is found that the material of region II is anisotropic and the radial refractive index is close to zero. However, such an anisotropic material is very difficult for realization, and we need to simplify the material parameters in Equation (1). Importantly, numerical results demonstrate that the far-field pattern is nearly invariant with the change of the radial refractive index (see Figure S1a in Supporting Information). Thus we

Dr. W. X. Jiang, Q. Cheng, H. F. Ma, Prof. T. J. Cui
State Key Laboratory of Millimeter Waves
Department of Radio Engineering
Southeast University
Nanjing 210096, China
E-mail: tjcui@seu.edu.cn
Prof. C.-W. Qiu, Dr. T. C. Han
Department of Electrical and Computer Engineering
National University of Singapore
Singapore 119620
E-mail: chengwei.qiu@nus.edu.sg
Prof. S. Zhang
School of Physics and Astronomy
University of Birmingham, UK

DOI: 10.1002/adma.201303657

ADVANCED MATERIALS
www.advmat.de

www.MaterialsViews.com

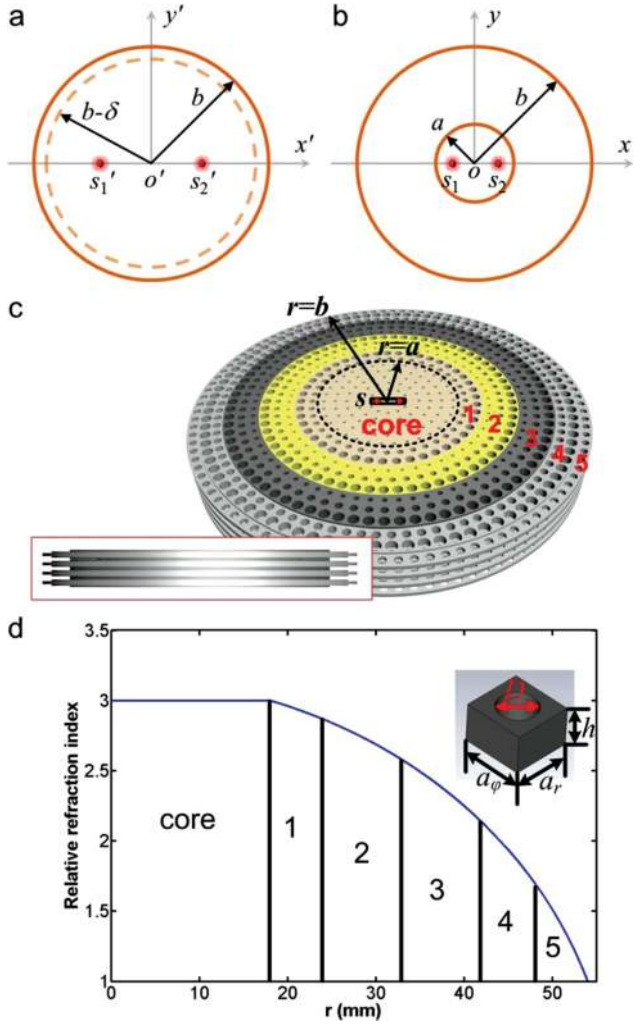

Figure 1. The schematic of magnifying lens and its simplification. (a–b) The schematic illustration of coordinate transformation for the design of modified solid immersion lens. The far-field patterns of two sources (s1 and s2) in the real space (Figure b) is equivalent to two sources (s1' and s2') in the virtual space (Figure a). (c) The schematic and realization of the simplified modified solid immersion lens, which is composed of isotropic dielectrics. The inset is the side view of the modified solid immersion lens. The modified solid immersion lens includes two parts: the central core with homogeneous material and the matching layer with gradient index materials. In the center of the core, there is a slot surrounded by boundary *s* to place sources denoted by two red points. (d) The effective parameters of the modified solid immersion lens. In the core region, the refractive index is 3. In the matching region, the refractive index ranges from 3 to 1 (free space).

can simply make $n_r = n_\phi = b/r$, and finally we obtain an isotropic modified solid immersion lens as

$$n(r) = \begin{cases} b/a & r \le a \\ b/r & a < r \le b. \end{cases} \quad (2)$$

Interestingly, we find that Equation (2) has a similar expression to the experienced formula in Ref. [15] Our further study shows that the isotropic modified solid immersion lens in Equation (2) is also effective for the transverse magnetic polarization (see Figure S1b). Thus the proposed modified solid immersion lens is independent of the polarization.

Since the modified solid immersion lens is made of inhomogeneous isotropic material, it can be generated by full dielectrics with the broadband performance. The modified solid immersion lens is schematically illustrated in Figure 1c, which includes two parts: region I is the core region, while region II is physically the impedance- matching layer. The role of the core region is to generate subwavelength propagation mode and the matching layer effectively transmits the sub-resolution information into the free-space propagating waves. From Equation (2), we observe that the refractive index of the matching layer changes adiabetically from $n_c = b/a$ to 1 (free space). Compared to the well-studied solid-immersion lenses,[22–24] the modified solid immersion lens here will transmit the signature of the sources more efficiently to the far field due to the impedance-matching layer. This is guaranteed approximately by the transformation-optics theory. The material profile of the modified solid immersion lens is demonstrated in Figure 1d, in which we set a = 18 mm and b = 54 mm. The sources to be imaged are embedded in the modified solid immersion lens by engraving a small air opening in the core center.

We first numerically validate the modified solid immersion lens performance. We set a = 18 mm, b = 54 mm, the operating frequency f_0 = 10GHz, the distance between two line sources d = 7.5 mm, and the relative permittivity in the core region $\varepsilon_c = n_c^2 = 9$. Note that the distance of two sources is about 0.25 wavelengths, which is far below the Abble diffraction limit. **Figures 2**a and 2b show the simulation results of two sources in the free space with small distance d and large distance $3d$, respectively. The left panel of Figure 2a illustrates the near-field distribution, which is similar to that of a single monopole antenna in two dimensions due to the deep subwavelength separation between the two sources. As we see in the right panel of Figure 2a, the field intensity along a circle with radius 60mm is nearly homogeneous, behaving as a monopole. In such a case, two sources are very difficult to be distinguished, i.e., they look like a single source in the far-field region. To distinguish the two sources, we have to enlarge their distance to at least half wavelength without the help of any lenses based on the Abbe diffraction limit. We present the near-field distributions of the two sources with enlarged distance $3d$ (0.75 wavelength) in the left panel of Figure 2b, which is remarkably different from that of single source. Along the same observation distance, the field amplitude changes significantly. In the left panel of Figure 2c, we illustrate the near-field distribution of two sources with small distance d inside the modified solid immersion lens, which shows very similar features as the left panel of Figure 2b. We also plot the field intensity along the observation circle in the right panel of Figure 2c, which is almost identical to the right panel of Figure 2b. Hence, with the proposed modified solid immersion lens, two sources with a deep subwavelength separation can be easily differentiated beyond the stipulated diffraction limit. To verify the far-field effect of the fabricated modified solid immersion lens, we also compute the radiation patterns, as shown in **Figure 3**b. We observe that the subwavelength-distance sources inside the modified solid immersion lens have equivalent far-field signatures to the large-distance sources in the free space.

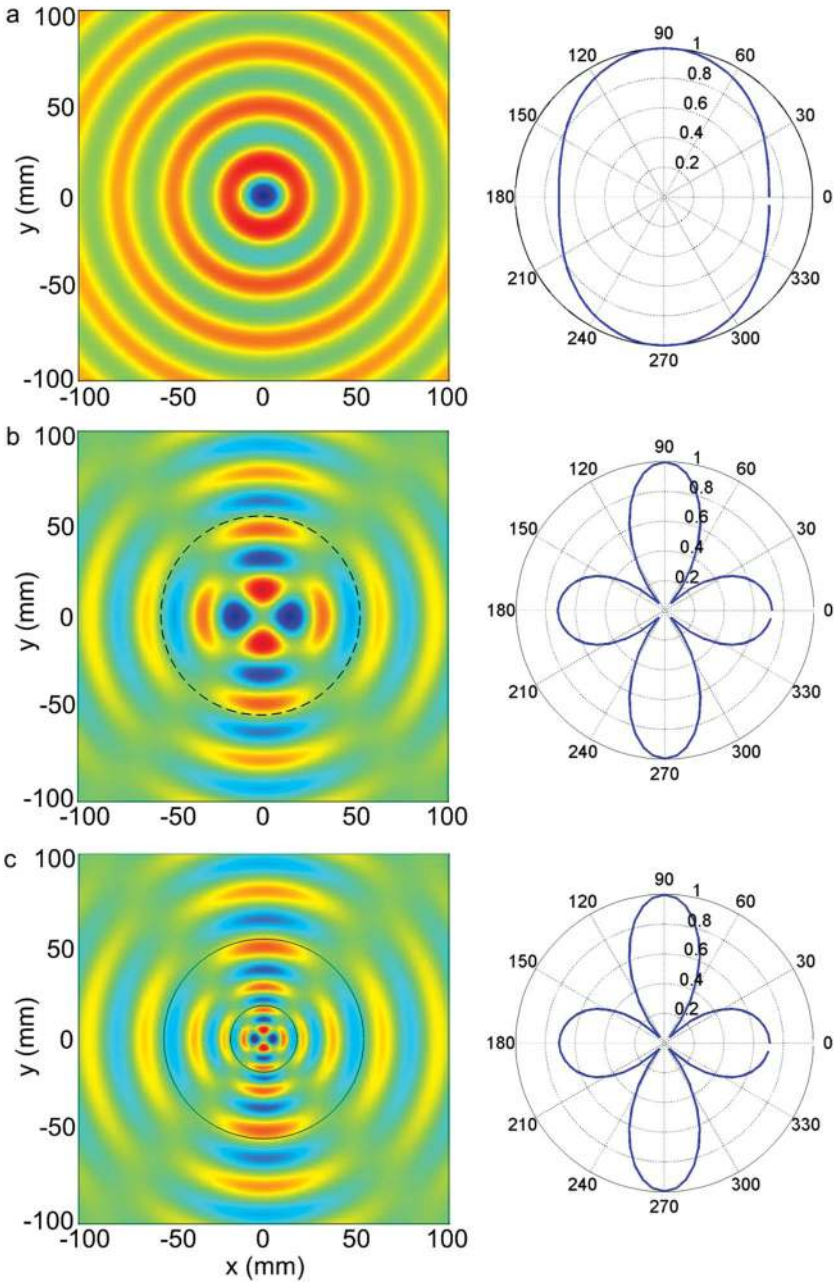

Figure 2. The simulation results of the designed magnifying (a modified type of solid immersion) lens at 10 GHz. (a) The near-field distribution of two sources with small distance (7.5 mm) in free space (the left panel), and the field intense along an observation circle with radius 60mm (the right panel). (b) The near-field distribution of two sources with large distance (22.5 mm) in free space (the left panel), and the field intense along the observation circle (the right panel). (c) The near-field distribution of two sources with small distance (7.5 mm) inside the modified solid immersion lens (the left panel), and the field intensity along the observation circle (the right panel).

The material parameters of the modified solid immersion lens are nonmagnetic, isotropic and inhomogeneous, which can be realized by non-resonant metamaterials. We fabricate the metamaterials using multi-layered dielectric plates by drilling spatially inhomogeneous air holes (Figure 3c) to achieve the gradient distribution of refractive indices (Figure 1d). Figure 3 illustrates the schematic and fabricated sample of the modified solid immersion lens. Three kinds of dielectric materials are involved in the lens' realization: the TP2 dielectric, which has large permittivity of 9.6 (with loss tangent 0.03), the FR4 dielectric, which has relatively large permittivity of 4.4 (with loss tangent 0.025), and the F4B dielectric, which has small permittivity of 2.65 (with loss tangent 0.003). We design the modified solid immersion lens to work in a broadband from 7 to 10 GHz, and choose five kinds of unit cells as the building blocks of the metamaterials to realize the required distribution of refractive index. The size of unit cell is $a_r \times a\varphi \times h$ mm^3. We choose the commercially available 3mm-thick TP2 plates, 3 mm-thick FR4 plates, 3mm-thick F4B plates, 2 mm-thick F4B plates, and 1mm-thick F4B plates to generate the five kinds of unit cells, respectively. The gradient variation of the refractive index (n) shown in Figure 1b can be obtained by changing the diameter (D) of the drilling air holes in unit cells.

The effective indices of refraction for above unit cells have been obtained using the effective medium theory and the S-parameter retrieval method.[25] For the two-dimensional case, such unit cells are isotropic due to the rotational symmetry. For the three-dimensional case, the nearly isotropic properties of unit cells have been studied in Ref. [26] by considering three orthogonal polarizations of incident waves. Hence, our impedance-matching magnifying lens may extend to three-dimensional space for practical applications. To verify the effective medium parameters of the drilling-hole unit cells, we simulate the near-field distribution of the structured modified solid immersion lens in Figure 3a, which is exactly the same as that of the continuous modified solid immersion lens in Figure 2c.

In real fabrications, the modified solid immersion lens is composed of four layers of the same structures, in which each layer is composed of the core region and the matching region. We divide the matching region into five subregions. The details of the effective medium parameters and the sizes of unit cells in each subregion are illustrated in Table S1 (see Supporting Information). The whole modified solid immersion lens is achieved by fixing the five parts together, as displayed in Figure 3c.

In experiments, a near-field scanning system is employed to measure the two-dimensional electric-field distributions. The upper and lower parallel metallic plates form a microwave planar waveguide, which ensures transverse electric mode as the dominant mode. A monopole probe is mounted in the upper plate to detect the electric-field distribution. In order to

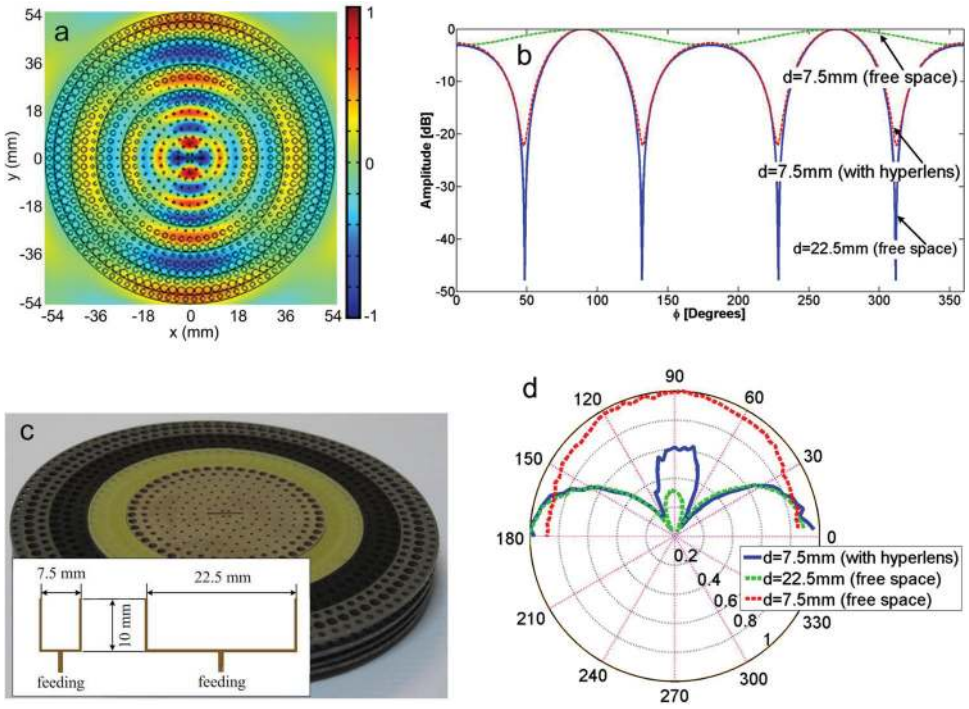

Figure 3. (a) The simulated field distribution inside the magnifying lens with hole-drilling dielectric structures. (b) The simulated far-field patterns of the modified solid immersion lens at 9 GHz. (c) The photograph of the fabricated magnifying lens. The inset is the designed power divider and two sources in experiments. (d) The measured field intensities (normalized) along the observation circle with radius of 60mm at 9 GHz, for two small-distance sources in free space (red dashed line), two large-distance sources in free space (green dashed line), and two small-distance sources inside modified solid immersion lens (blue solid line).

obtain two feeding sources, we design a simple power divider upon the lower plate, shown in inset of Figure 3c. Following the numerical simulations, the distance of two small-distance sources is 7.5 mm, and the distance of two large-distance sources is 22.5 mm. Such two feeding sources are embedded into a slot in the modified solid immersion lens center. With this slot, the sources will be immersed in the magnifying lens and hence it is also termed the "modified solid immersion lens". A moving stage has been used to carry the lower metallic plate and scans in the x and y directions, so that we can measure the near-field distributions in a certain area. The step resolution in both scanning directions is set as 1 mm. Due to the symmetry of the modified solid immersion lens and two sources, only half region is mapped.

To validate the designed impedance-matching magnifying lens experimentally, we measure the fabricated sample which has the same geometrical size as that in simulations (a = 18mm, b = 54 mm, and d = 7.5 mm) in broadband from 7 GHz to 10 GHz. Note that, at 10 GHz, the small distance (d) of two sources is 0.25 wavelength and the large distance ($3d$) is 0.75 wavelength; while at 7 GHz, the small distance is 0.175 wavelength and the large distance is 0.525 wavelength. **Figure 4** illustrates the measured results of two small-distance and two large-distance sources, respectively. The first row shows the near-field distributions of two small-distance sources without modified solid immersion lens at 7 GHz (Figure 4a1), 8 GHz (Figure 4b1), 9 GHz (Figure 4c1), and 10 GHz (Figure 4d1). In this case, the distance of two sources is much smaller than the diffraction limit, and hence the near field is very similar to that of a single source. That is to say, the sources are very difficult to be distinguished. When the two small-distance sources are enclosed by the modified solid immersion lens, however, the field distributions are changed to nearly the same as those of two sources at large distance ($3d$) in free space, as demonstrated in the second and third rows of Figure 4. We notice that the two sources can be evidently distinguished. To illustrate the effect of the modified solid immersion lens quantitatively, we also plot the normalized measured field intensity along a circle with radius 60 mm at 9 GHz in Figure 3d. It is obvious that the radiation of two small-distance sources is almost isotropic. However, the radiation of the same small-distance sources within the modified solid immersion lens is nearly the same as that of two large-distance sources, and hence they can be distinguished by the outer detectors. It can be seen that the performance of the modified solid immersion lens is very good in a broad frequency band. Therefore, the super-resolution and broadband properties are reached simultaneously in the proposed modified solid immersion lens.

For practical applications, it is important to be able to deduce the configuration of the sources embedded in the modified solid immersion lens based on the recorded far-field radiation patterns. We have developed an inversion scheme to determine the positions of sources from far fields (see Supporting Information). We consider two examples with different distances between the two sources. The results are demonstrated in **Figure 5**. In both examples, the magnification factor of the modified solid immersion lens is 3. For the two

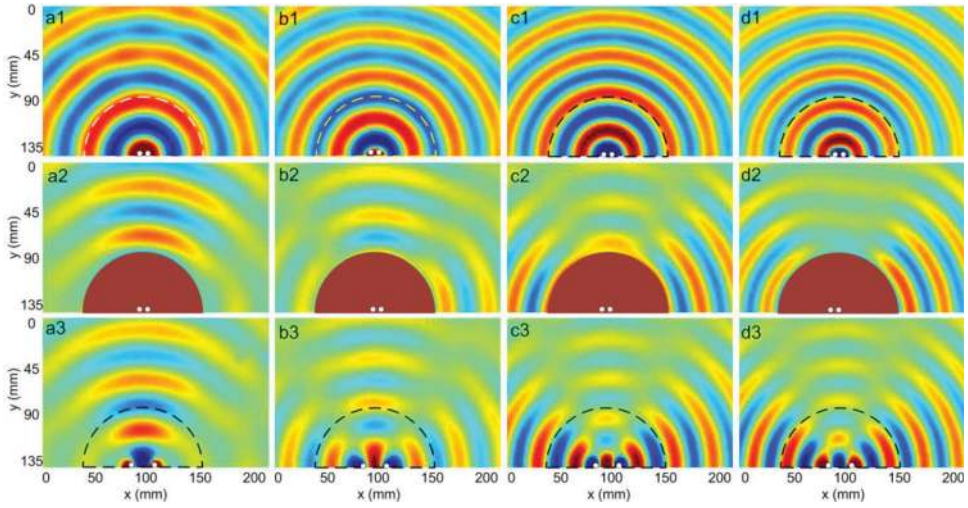

Figure 4. The measured field distributions of the magnifying lens. The first rows (a1,b1,c1,d1) show the results of two sources with small distance (7.5 mm) in free space at different frequencies. The second rows (a2,b2,c2,d2) show the results of two sources with small distance (7.5 mm) inside the modified solid immersion lens at different frequencies. The third rows (a3,b3,c3,d3) show the results of two sources with large distance (22.5 mm) in free space at different frequencies. The first to fourth columns indicate the results of 7, 8, 9, and 10 GHz, respectively. The comparison of the second and third rows illustrates the broadband performance of the modified solid immersion lens. The two white points in each subfigure denote the two sources in experiments.

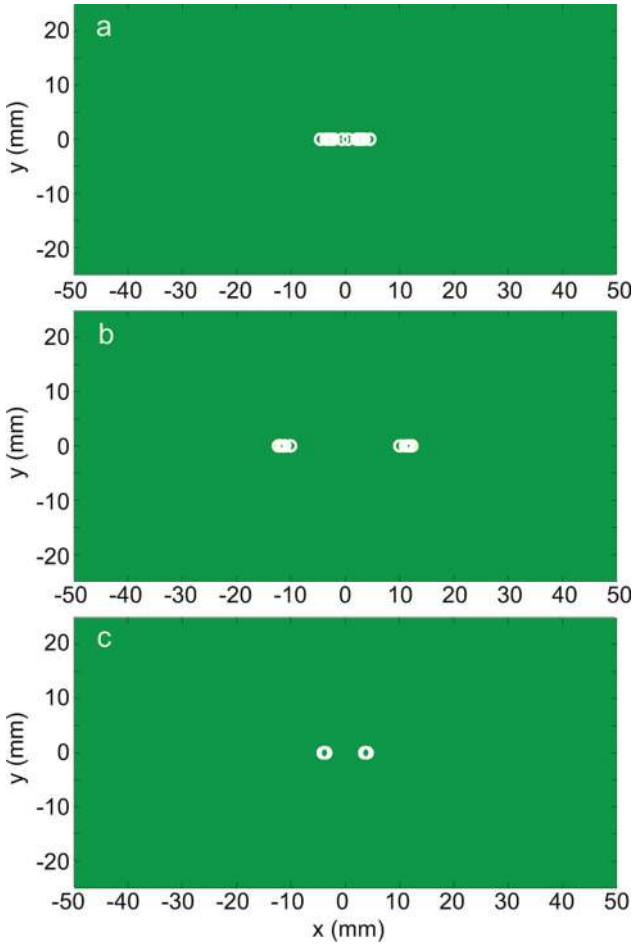

Figure 5. The retrieved locations of sources with white noise considered. (a) Two sources in free space with 7.5 mm distance at 10 GHz. (b) Two sources in free space with 22.5 mm distance at 10 GHz. (c) Two sources inside the modified solid immersion lens with 7.5 mm distance at 10 GHz.

7.5mm-distance sources in free space, the retrieved locations of two sources are difficult to be distinguished, as shown in Figure 5a. However, when such two sources are placed in the graded magnifying lens, their physical positions can be clearly identified, as displayed in Figure 5c. For the two sources with 22.5 mm separation in free space, the retrieved positions are distinctly perceived (see Figure 5b) since they are beyond the diffraction limit. We note that breaking the diffraction limit is possible by retrieving the position of point sources from the far field without any noise. However, when we add some white noise to the radiation information, the location of the sources can hardly be distinguished as shown in Figure 5a.

In conclusion, we have proposed a transformation-optics modified solid immersion lens and fabricated a microwave sample using the full-dielectric metamaterial. The experimental results have verified the super-resolution performance of the dielectric modified solid immersion lens in broadband from 7 to 10 GHz. Owing to the low loss and broadband properties, this modified solid immersion lens can be used to far-field imaging with high resolution that could be captured directly by a conventional microwave imaging device. Unlike the method of far-field time-reversal mirror,[18–21] which is made of antenna array and dependent on post signal processing, the presented modified solid immersion lens is composed of graded dielectrics with extremely low loss.

Supporting Information

Supporting Information is available from the Wiley Online Library or from the author.

Acknowledgements

W.X.J., C.-W.Q. and T.C.H. contributed equally to this work. We acknowledge the supports in part by the National Science Foundation of China under Grant Nos. 60990320, 60990321, 60990324, 61171024,

61171026, and 61138001, in part by the National High Tech (863) Projects under Grant Nos. 2011AA010202 and 2012AA030402, in part by the 111 Project under Grant No. 111–2–05, and in part by the Fundamental Research Funds for the Central Universities. C.-W.Q. acknowledges the support from the National University of Singapore under Grant No. R-263–000–688–112 and T.C.H. acknowledges the support from National Science Foundation of China under Grant No. 11304253.

Received: August 6, 2013
Published online: September 23, 2013

[1] M. Born, E. Wolf, *Principles of Optics*, Cambridge University Press, Cambridge, **1999**.
[2] J. B. Pendry, *Phys. Rev. Lett.* **2000**, *85*, 3966.
[3] N. Fang, H. Lee, C. Sun, X. Zhang, *Science* **2005**, *308*, 534.
[4] T. Taubner, D. Korobkin, Y. Urzhumov, G. Shvets, R. Hillenbrand, *Science* **2006**, *313*, 1595.
[5] X. Zhang, Z. W. Liu, *Nat. Mater.* **2008**, *7*, 435.
[6] Z. W. Liu, et al. *Nano lett.* **2007**, *7*, 403.
[7] Z. Jacob, L. V. Alekseyev, E. Narimanov, *Opt. Express* **2006**, *14*, 8247.
[8] A. Salandrino, N. Engheta, *Phys. Rev. B* **2006**, *74*, 075103.
[9] I. I. Smolyaninov, Y. J. Huang, C. C. Davis, *Science* **2007**, *315*, 1699.
[10] Z. W. Liu, H. Lee, Y. Xiong, C. Sun, X. Zhang, *Science* **2007**, *315*, 1686.
[11] J. Rho, et al. *Nat. Commun.* **2010**, *1*, 143.
[12] U. Leonhardt, *Science* **2006**, *312*, 1777.
[13] J. B. Pendry, D. Schuring, D. R. Smith, *Science* **2006**, *312*, 1780.
[14] M. Tsang, D. Psaltis, *Phys. Rev. B* **2008**, *77*, 035122.
[15] B. L. Zhang, G. Barbastathis, *Opt. Express* **2010**, *18*, 11216.
[16] U. Leonhardt, *New J. Phys.* **2009**, *11*, 093040.
[17] Y. G. Ma, S. Sahebdivan, C. K. Ong, T. Tyc, U. Leonhardt, *New J. Phys.* **2012**, *14*, 025001.
[18] G. Lerosey, J. de Rosny, A. Tourin, M. Fink, *Science* **2007**, *315*, 1120.
[19] F. Lemoult, G. Lerosey, J. de Rosny, M. Fink, *Phys. Rev. Lett.* **2010**, *104*, 203901.
[20] F. Lemoult, M. Fink, G. Lerosey, *Phys. Rev. Lett.* **2011**, *107*, 064301.
[21] F. Lemoult, M. Fink, G. Lerosey, *Nat. Comm.* **2012**, *3*, 889.
[22] Q. Wu, G. D. Feke, D. Grober, L. P. Ghislain, *Appl. Phys. Lett.* **1999**, *75*, 4064.
[23] S. M. Mansfield, G. S. Kino, *Appl. Phys. Lett.* **1990**, *57*, 2615.
[24] B. D. Terris, H. J. Mamin, D. Rugar, W. R. Studenmund, G. S. Kino, *Appl. Phys. Lett.* **1994**, *65*, 388.
[25] D. R. Smith, S. Schultz, P. Markos, C. M. Soukoulis, *Phy. Rev. B* **2002**, *65*, 195104.
[26] H. F. Ma, T. J. Cui, *Nat. Comm.* **2010**, *1*, 124.